JCI The Journal of Clinical Investigation

Modulating fast skeletal muscle contraction protects skeletal muscle in animal models of Duchenne muscular dystrophy

Alan J. Russell, … , Leslie A. Leinwand, Kevin Koch

J Clin Invest. 2023. https://doi.org/10.1172/JCI153837.

Research In-Press Preview Muscle biology Therapeutics

Graphical abstract

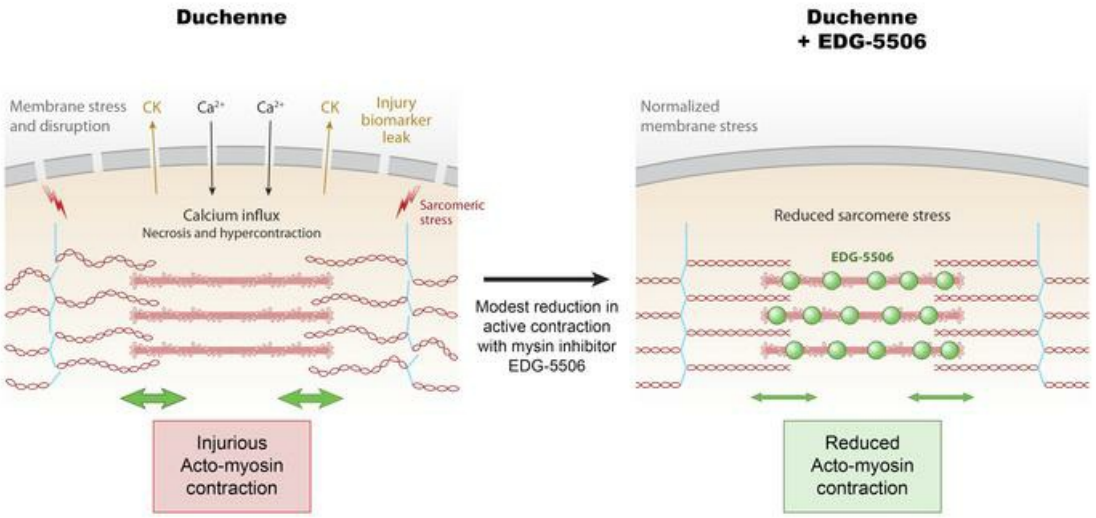

Title page

Modulating fast skeletal muscle contraction protects skeletal muscle in animal models of Duchenne muscular dystrophy.

Authors: Alan J Russell[1*], Mike DuVall[1], Ben Barthel[1], Ying Qian[1], Angela K. Peter[1], Breanne L. Newell-Stamper[1], Kevin Hunt[1], Sarah Lehman[1], Molly Madden[1], Stephen Schlachter[1], Ben Robertson[1], Ashleigh Van Deusen[1], Hector M Rodriguez[2], Carlos Vera[3], Yu Su[4], Dennis R Claflin[5], Susan V Brooks[4], Peter Nghiem[6], Alexis Rutledge[6], Twlya I Juehne[7], Jinsheng Yu[7], Elisabeth R. Barton[8], Yangyi E Luo[8], Andreas Patsalos[9], Laszlo Nagy[9], H Lee Sweeney[10], Leslie A Leinwand[3] and Kevin Koch[1]

Affiliations:

[1]Edgewise Therapeutics, BioFrontiers Institute, University of Colorado, Boulder, CO 80303, USA.

[2]BridgeBio Inc., 421 Kipling Street, Palo Alto, CA 94301, USA.

[3]Department of Molecular, Cellular, and Developmental Biology and BioFrontiers Institute, University of Colorado, Boulder, CO 80309, USA.

[4]Molecular and Integrative Physiology, University of Michigan, 2029 BSRB, Ann Arbor MI 48109, USA.

[5]Department of Surgery, Section of Plastic Surgery, University of Michigan, Ann Arbor MI 48109, USA.

[6]Department of Veterinary Integrative Biosciences, College of Veterinary Medicine and Biomedical Sciences, Texas A&M University, College Station, TX 77843, USA.

[7]Genome Technology Access Center, Department of Genetics, Washington University in Saint Louis School of Medicine, 660 S. Euclid Ave. Campus Box 8232, Saint Louis, MO, USA.

[8]Department of Applied Physiology and Kinesiology and Myology Institute, University of Florida College of Health and Human Performance, Gainesville, Florida, USA

[9]Departments of Medicine and Biological Chemistry, Johns Hopkins University School of Medicine, Institute for Fundamental Biomedical Research, Johns Hopkins All Children's Hospital, St. Petersburg, FL, USA.

[10]Department of Pharmacology and Therapeutics and Myology Institute, University of Florida College of Medicine, Gainesville, Florida, USA.

*Correspondence to: arussell@edgewisetx.com, Edgewise Therapeutics, 1715 38th Street Boulder 80301.

Competing interests: Alan Russell, Mike DuVall, Ben Barthel, Ying Qian, Angela Peter, Breanne Newell-Stamper, Kevin Hunt, Stephen Schlachter, Ben Robertson, Ashleigh Van Deusen and Kevin Koch are employees of and own stock or options to purchase stock for Edgewise Therapeutics. Leslie A Leinwand and H Lee Sweeney are scientific advisors for Edgewise Therapeutics and own options to purchase stock.

Keywords: Muscular dystrophy, dystrophin, fast myosin, eccentric injury, protection

Total Word Count 10,727 (main doc minus supps). This PDF file includes:

Main Text
Figures 1 to 7
Supplementary Table 1 to 3
Supplementary Figures 1 to 7

Abstract

Duchenne muscular dystrophy (DMD) is a lethal muscle disease caused by absence of the protein dystrophin, which acts as a structural link between the basal lamina and contractile machinery to stabilize muscle membranes from mechanical stress. In DMD, mechanical stress leads to exaggerated membrane injury and fiber breakdown, with fast fibers being the most susceptible to damage. A major contributor to this injury is muscle contraction, controlled by the motor protein myosin. However, the relationship between how muscle contraction and fast muscle fiber damage contribute to the pathophysiology of DMD has not been well characterized. We explored the role of fast skeletal muscle contraction in DMD with a novel, selective, orally active inhibitor of fast skeletal muscle myosin, EDG-5506. Surprisingly, even modest decreases of contraction (<15%) were sufficient to protect skeletal muscles in dystrophic *mdx* mice from stress injury. Longer-term treatment also decreased muscle fibrosis in key disease-implicated tissues. Importantly, therapeutic levels of myosin inhibition with EDG-5506 did not detrimentally affect strength or coordination. Finally, in dystrophic dogs, EDG-5506 reversibly reduced circulating muscle injury biomarkers and increased habitual activity. This unexpected biology may represent an important alternative treatment strategy for Duchenne and related myopathies.

Brief Summary

Exploration of the relationship between contraction of dystrophic skeletal muscle and degeneration with a novel, selective myosin inhibitor reveals unexpected protective effects.

Main Text

Introduction

DMD is a lethal, inherited muscle myopathy caused by the absence of dystrophin and destabilization of the dystrophin-glycoprotein complex (DGC) in the cell membrane (1). Dystrophin provides a structural link between the contractile elements of the sarcomere and the basement membrane of muscle (2). When dystrophin is dysfunctional, mechanical stress (force applied over

the muscle area) can lead to the opening of membrane stress channels (such as the TRPC family) and the influx of calcium (3). Ectopic calcium initiates muscle fiber breakdown through several mechanisms including hypercontraction, activation of proteases, and initiation of mitochondrial apoptotic and necrotic pathways (4). Once muscle fiber breakdown has occurred, skeletal muscle regeneration is possible through the activation of inflammatory pathways and mobilization of muscle stem cells. However, chronic inflammation, cell stress and stem cell exhaustion reduce the fidelity of this process as DMD patients get older, leading to fatty and fibrotic tissue accumulation within muscle and compromised physical function (5). Continued muscle degeneration eventually leads to mortality by either cardiac or respiratory muscle failure by the third to fourth decade of life (6).

The connection between mechanical stress and muscle breakdown in DMD has been the source of scientific research for several decades. Dystrophin is not required for normal sarcomeric organization and contractile activity, as experiments in isolated fibers using dystrophic *mdx* mouse muscle where membranes have been removed demonstrate normal force and injury resistance. In contrast, contraction of intact *mdx* muscle causes sarcolemmal rupture and force loss (7), particularly under lengthening (eccentric) conditions. Passive lengthening is not sufficient to yield exaggerated injury (8) and removal of contraction by denervation (9), or treatment with high concentrations of the myosin inhibitor, N-benzyl-p-toluene sulphonamide (BTS) also prevent injury (10). The specific nature of structural rearrangements caused by contraction that lead to membrane stress and degeneration in dystrophic muscle is not currently understood.

Adult skeletal muscle consists of two main fiber types, ‘slow’ (type I) and ‘fast’ (types IIa and IIx/d; type IIb is also present in other mammals but not human muscle), defined by the myosin isoform that they express (11). Muscles enriched in fast fibers are more susceptible to mechanical stress in dystrophic mice while muscles enriched with slow fibers are more resistant (12). This also appears to be the case in individuals with DMD. Histological studies of young DMD patients display fiber-type imbalances in the co-localization of fast and embryonic myosin, a marker of regenerating muscle fibers (13). Circulating biomarkers of muscle injury specific to fast but not slow fibers, such

as fast troponin I are also enriched in the plasma of DMD individuals (14). Histological observations of fast fiber susceptibility have also been made in dog and pig models of DMD (15, 16). With age, slow skeletal muscle fibers also show evidence of injury, including co-expression of embryonic myosin (17). The cause of fast fiber susceptibility to injury and whether it has any influence on slow fiber injury or overall progression of disease is not well understood.

In this study, we used a pharmacological approach to explore the role of muscle fiber contraction in dystrophic muscle stress and degeneration. To achieve this goal, we developed a compound, EDG-5506, which inhibits the ability of myosin to hydrolyze ATP and develop force by decreasing strong binding between myosin and actin within the sarcomere. The high selectivity of this compound for fast but not slow skeletal, cardiac, or smooth muscle also allowed us to dissect the role of fast muscle contraction in muscle breakdown and disease progression in models of DMD. Using EDG-5506 ex vivo, in situ and in vivo, we come to the unexpected conclusion that small amounts of fast myosin inhibition result in almost complete protection against skeletal muscle membrane injury, force loss and longer-term fibrosis. These results point to the possibility that fast myosin inhibition may represent an alternative treatment modality for DMD and other myopathies that are exacerbated by mechanical stress.

Results

Contraction via fast skeletal myosin is coupled to force drop and membrane injury in dystrophic muscle.

To explore the contribution of skeletal muscle contraction to injury in dystrophic muscle, we sought to identify an inhibitor of skeletal contraction that was appropriate for both in vitro and in vivo experiments and was not inhibitory to cardiac or smooth muscle. Contraction of muscle is directly coupled to ATP hydrolysis (18) so we used a high-throughput small molecule screen measuring fast skeletal muscle myofibril ATPase to identify promising leads (Supplemental figure 1A). Chemical leads were optimized for potency, selectivity, physiochemical and pharmacokinetic

properties, leading to the identification of EDG-5506 (Figure 1A). The inhibitory activity and specificity of EDG-5506 was measured using myofibril preparations of different myosin composition. EDG-5506 completely inhibited fast myofibril ATPase from rabbit psoas muscle (96% IIx/d (19)) with an IC_{50} of 0.2 μM but was inactive against cardiac and slow bovine masseter skeletal myofibrils (100% type I) with an IC_{50} greater than 100 μM (Figure 1B). EDG-5506 was also a potent inhibitor of other mixed fast myosin myofibrils (mouse gastroc IC_{50} 0.4 μM, 21% IIa, 15% IIx, 56% IIb; mouse TA IC_{50} 0.4 μM, mixed IIa, IIx, IIb (20), Supplemental Figure 1B) suggesting equal potency against all fast skeletal myosin proteins. In contrast, EDG-5506 was a partial inhibitor of mixed-composition fast/slow human muscle myofibrils (Supplemental Figure 1C, additional selectivity data Supplemental Table 1). In addition to EDG-5506, we also developed a second myosin inhibitor, EDG-4131 for confirmation of results (details of the structure and biochemical activity of EDG-4131, Supplemental Figure 1D, Supplemental Table 2).

The complex nature of these muscle preparations does not allow determination of compound mechanism. Myosin inhibition was confirmed by measuring the actin-activated ATPase of a purified S1 myosin motor sub-fragment (21). EDG-5506 inhibited the enzymatic activity of fast skeletal S1 from rabbit psoas but not porcine ventricular cardiac S1 or the more unrelated smooth muscle S1 with an IC_{50} of 0.11 μM and >100 μM, respectively (Figure 1C). Other myosin inhibitors, including fast-selective BTS (22) and cardiac-selective mavacamten (23), inhibit inorganic phosphate (Pi) release, the rate-limiting step in the actin-myosin ATPase cycle (Supplemental Figure 1E). We compared the effect of EDG-5506 and BTS on Pi release with actin. Preincubation of EDG-5506 or BTS and myosin (minus nucleotide) for 30 mins prior to addition of actin decreased the rate of Pi release (Supplemental Figure 1F).

The specificity of EDG-5506 for fast skeletal myosin over other, unrelated proteins was confirmed using two off-target binding and activity screens. EDG-5506 (at 20 μM) did not exhibit any binding affinity with 90 kinase proteins in vitro (KINOMEscan™, Eurofins DiscoverX, San Diego, CA). A second off-target panel (SAFETYscan E/IC_{50} ELECT, Eurofins DiscoverX, San Diego, CA) tested in vitro enzyme activity against 78 proteins including GPCR, ion channel, kinases, nuclear hormone

receptors and transporters. In all assays, the IC_{50} of EDG-5506 was >10 μM (Supplemental Data 1).

We next tested the ability of EDG-5506 to reduce force in intact muscle. In detergent-treated single fiber preparations (24), EDG-5506 selectively reduced force in fast rabbit psoas muscle fibers (Figure 1D) with an IC_{50} of 0.7 μM (Supplemental Figure 1G). In contrast, EDG-5506 had no effect on slow skeletal rat soleus (100% type I) or rat cardiac muscle fibers (Supplemental Figure 1H, 1I). In ex vivo assays using mouse extensor digitorum longus (EDL, 100% fast, majority IIb myosin (20, 25)), EDG-5506 reduced force in a concentration and time-dependent manner, completely inhibiting force at 10 μM (Figure 1E). Submaximal force was also similarly inhibited (Supplemental Figure 1J). Similar experiments with mixed fast/slow mouse soleus (31% type I, 60% type IIa/IIx (20)) muscle yielded partial force inhibition (Supplemental Figure 1K).

EDL muscles from *mdx* mice have an exaggerated injury response to lengthening (eccentric) contraction, exhibiting strength loss with repeated contractions (8). EDL muscles were pre-incubated with EDG-5506 and peak strain and strength loss was measured over ten rounds of lengthening contractions (Supplemental Figure 2A). EDG-5506 lowered pre-injury isometric force and lengthening peak strain in a concentration-dependent manner in both *mdx* and WT muscle (Figure 2A). Inhibition of peak strain was less than isometric force, leading to an increase in the eccentric:isometric force ratio with EDG-5506 (Supplemental Figure 2B). Strength drop with repeated contractions in *mdx* muscle was dramatically lowered with EDG-5506 (Figure 2B, 2C), protecting against isometric and peak force drop (Figure 2D, 2E). Both metrics approached but did not achieve WT strength drop, perhaps suggesting other contributing factors. The dose response for protection had a surprisingly non-linear relationship with near maximal protection at ≤1 μM, a concentration associated with approx. 15% inhibition of isometric force (Figure 2A). Similar protection was also observed with EDG-4131 (Supplemental Figure 2C). Several signaling pathways have been implicated in protection from eccentric injury including Akt (26), IGF1 (27) and LTBP4/TGFβ (28). To assess whether any of these pathways were directly or indirectly modulated by EDG-5506, EDL muscle from *mdx* mice was incubated with vehicle or 5 μM EDG-5506 for 1 hr

prior to analysis with a phosphoprotein array. There were no consistent changes in implicated pathways (Supplemental Data 2).

We next examined muscle responses in situ, measuring mouse TA muscle force after stimulation of the sciatic nerve, with a two-contraction lengthening injury model (29). Oral administration of EDG-5506 decreased isometric force in a dose-dependent manner (Figure 2F, Supplemental Figure 2D). Lengthening injury yielded an exaggerated strength drop in *mdx* but not WT TA muscle which was dramatically improved in *mdx* with EDG-5506 (Figure 2G). Like ex vivo results, protection was achieved at doses associated with small decreases in isometric force (<10%), with force drop similar to WT mice. Protection was specific to dystrophic muscle as there was no decrease in force drop in WT mice (Figure 2G). Unlike ex vivo results, lengthening peak stress was not altered by treatment (Supplemental Figure 2E). EDG-4131 was also protective against in situ injury (Supplemental Figure 2F). Muscle injury is commonly associated with increased circulating creatine kinase (CK). Treatment of *mdx* mice with EDG-5506 prior to in situ injury lowered plasma CK activity compared to control mice (Figure 2H). There was no short-term effect of EDG-5506 on CK in the absence of lengthening injury (Supplementary figure 2G).

Membrane stress is an important component of eccentric injury in dystrophic muscle (30). We next performed ex vivo lengthening contraction of *mdx* EDL muscle using a membrane-impermeable dye to assess sarcolemmal disruption. EDG-5506 effectively reduced dye uptake (Figure 3A, 3B). There was no effect of the dye itself on force (Supplemental Figure 3A). One consequence of membrane disruption is extracellular calcium uptake, a major contributing factor to muscle fiber necrosis (4). We used an ex vivo mouse lumbrical model (31) with fura-2 calcium indicator dye to measure the effect of EDG-5506 on calcium dynamics and uptake with contraction in *mdx* lumbrical muscle. EDG-5506 reduced pre-injury force without altering calcium transients (Figure 3C, Supplemental Figure 3B). Contraction caused a strength drop that was completely prevented by EDG-5506 (Figure 3D). EDG-5506 also reduced accumulation of resting calcium and tension (Figure 3E, 3F, Supplemental Figure 3C). Calcium also drives destructive hypercontraction and clotting of fiber myoplasm (31). EDG-5506 completely prevented clot formation (Figure 3G, 3H,

Supplemental Movie 1-3). Highlighting the importance of calcium influx to muscle injury (32), we measured a linear relationship between inter-contraction calcium and force drop that was corrected with EDG-5506 (Supplemental Figure 3D). Consistent with previous results, maximal efficacy was achieved at 0.3 μM, where specific tension prior to injury was reduced by 15%.

EDG-5506 protects skeletal muscle in mdx and DBA/2 mdx mice in vivo

Mice have >90% fast muscle and its contraction is essential to physical activity (33). We next tested whether protective levels of myosin inhibition impaired strength, coordination, or activity in vivo. Single doses of EDG-5506 up to 10 mg/kg had no effect on grip strength or rotarod endurance in WT or *mdx* mice (Figure 4A). EDG-5506 also had no impact on wheel running (Supplemental Figure 4A). Physical exercise causes enhanced muscle injury in *mdx* mice, particularly with respect to plasma CK (34). We assessed plasma CK after strength and coordination tests. EDG-5506 treated *mdx* mice had significantly lower post-exercise CK compared to controls (Figure 4B). There was no effect of single doses of EDG-5506 on CK without exercise (Supplemental figure 4B). Membrane permeability can also be visualized in vivo via Evans blue dye (EBD) muscle uptake (35). Three weeks treatment of *mdx* mice with EDG-5506 reduced blue fibers close to that seen in WT mice, demonstrating muscle protection with longer compound treatment without formal exercise (Figure 4C, 4D, Supplemental Figure 4C).

Muscle degeneration in *mdx* mice leads to fibrosis, particularly in the diaphragm (36). We next tested whether chronic treatment with EDG-5506 would benefit fibrosis in *mdx* mice. Seven-week-old *mdx* mice were dosed with EDG-5506 for eight-weeks. EDG-5506 increased average grip strength (Figure 5A) and decreased diaphragm fibrosis compared to placebo (Figure 5B) and returned the skeletal muscle transcription profile closer to that of WT mice (Figure 5C, Supplemental Data 3). EDG-5506 had no effect on body or muscle weight and there was a trend towards fewer small, fragmented fibers in the TA muscle but not the diaphragm (Supplemental Figure 5A-5D). A rotarod test administered mid-study confirmed sustained membrane protection with decreased exercise-associated plasma CK (Supplemental Figure 5E). To better understand

the impact of EDG-5506 on muscle degeneration, we performed a second study in young *mdx* prior to muscle necrosis that peaks at weaning (3-4 weeks) with the soleus muscle particularly affected (37). EDG-5506 decreased central nucleation with a trend towards decreased embryonic myosin positive fibers in the soleus (Figure 5D). Specific tension was also higher in the soleus of treated WT and *mdx* mice (Figure 5E). Muscle size, fiber size and proportion of fast (IIA) fibers was unaffected (Supplemental Figure 5F, 5G, 5H).

Unlike DMD patients, *mdx* mice exhibit limited muscle fibrosis (36). Therefore, we performed studies in the more fibrotic DBA/2J *mdx* mouse (38). Beyond fibrosis, DBA/2J *mdx* also exhibit more fragmented, smaller fibers (39). EDG-5506 had no effect on body or muscle weights but the diaphragm muscle had fewer small fibers after 12-weeks dosing (Supplemental Figure 5I-5K). Treatment also reduced fibrosis in TA and diaphragm muscles with a trend towards lower fibrosis in the left ventricle (Figure 5F, 5G). Studies in DBA/2J *mdx* with EDG-4131 also confirmed this pattern, including significant decreases in left ventricular fibrosis (Supplemental Figure 5I-5M).

EDG-5506 lowers disease biomarkers and improves physical function in DMD dogs

We viewed data in mice as encouraging but were interested in testing EDG-5506 in dystrophic Golden Retriever (GRMD) dogs where muscle composition and function more closely resemble humans (40). Older (7 months), disease-stable GRMD were dosed in two-week periods with vehicle then EDG-5506 followed by a vehicle washout. As fast fiber atrophy has been documented in DMD dogs (16), we confirmed sustained fast myosin from biopsies of age-matched WT/GRMD gastrocnemius muscle (Supplemental figure 6A). EDG-5506 concentration was measured from a muscle biopsy at the end of the dosing period (4951 +/- 217 ng/g muscle). EDG-5506 administration was associated with a >50% decrease in CK, returning to pre-treatment levels after compound washout (Figure 6A). Physical activity normally increases CK in GRMD (41) raising the question whether EDG-5506 lowered CK via decreasing physical activity. We sought to test the effect of EDG-5506 on habitual activity in the same dogs using an activity monitor (42). EDG-5506 improved average daily activity by >30% (Figure 6B, Supplemental Figure 6B) with reversible increases in

time active and decreases in time resting (Figure 6C). One GRMD used in the biomarker study was too severely progressed to participate in this study. Activity in this dog did not change over the same dosing period (Supplemental Figure 6C*)*.

Somascan plasma proteomics has been used in DMD patients to generate a distinguishing protein signature vs healthy controls (43). As CK was decreased with EDG-5506, we asked whether other proteins associated with DMD were also changed. Somascan comparison of GRMD to healthy dog plasma revealed many protein differences (Supplemental Data 4). We examined the effect of EDG-5506 on the proteomic signature of GRMD. Treatment reversibly lowered GRMD-elevated proteins and increased GRMD-downregulated proteins (Figure 7A, Supplemental Data 5). Gene ontology (GO) term analysis revealed decreases in pathways associated with dystrophic muscle including apoptotic, cellular signaling, metabolic and immune responses (Supplemental table 3). Comparison of the GRMD proteomic signature with that from DMD (43) revealed a common set of 40 elevated and 9 depleted proteins (Figure 7B). EDG-5506 also significantly reversed this common DMD signature (Figure 7C, Supplemental Data 6).

Discussion

These studies reveal a surprising sensitivity of dystrophic muscle to sarcomeric and membrane stabilization by inhibition of force by fast skeletal muscle myosin. Following the experiments reported here, reports have also proposed fast myosin inhibition as a strategy for muscle relaxation in myotonia or spasticity (44). Our findings uncover a connection between muscle contraction and dystrophic muscle injury and expand the possible uses for this class of compounds into DMD, a progressive, grave disease. This relationship may also apply to other myopathies where muscle contraction causes fiber breakdown including types of limb girdle muscular dystrophy, Becker muscular dystrophy, and metabolic myopathies such as McArdle’s disease (45).

Protective effects from myosin inhibition build on earlier reports of dystrophic muscle protection by ablation of muscle contraction by unloading , denervation or immobilization with the myosin inhibitor

BTS (10). In contrast to these approaches, we demonstrate that full immobilization is not required for protection and that modest force inhibition (10-15%) is sufficient to prevent dystrophic muscle injury. Our initial assumption was that muscle protection via this mechanism would occur through decreased contraction peak strain, a key contributor to injury in dystrophic muscle (8, 30). These results question this hypothesis as EDG-5506 had only modest effects on peak strain ex vivo and no effect in situ. Examination of the ratio between isometric force and peak strain, another factor influencing dystrophic muscle injury (8), revealed an increase with treatment (Supplemental Figure 2C). This is consistent with reports showing decreased isometric force but increased force enhancement with lengthening in skeletal muscle fibers treated with myosin inhibitors such as BDM and vanadate (46, 47). Mechanistically, it has been proposed that inhibitors that increase the weak bound myosin ADP.Pi state convert to a strong bound state with lengthening. Functional consequences of this lengthening enhancement are unclear.

The magnitude of eccentric stress in our injury models is not commonly seen in sedentary mice, yet we measured significant decreases in Evans blue dye incorporation with EDG-5506. A hypothesis for protection in sedentary mice is based on an established model (31) where muscle fiber stress causes localized increases in calcium and non-uniform contraction of serial sarcomeres. In dystrophic muscle, the lack of costameres amplifies stress along serial sarcomeres resulting in further membrane stress and calcium entry. Under these conditions, EDG-5506 would provide protection against local stress by limiting uneven contraction.

A caveat with any small molecule approach is that off-target activities might contribute to positive pharmacology. Documented pathways that also confer protective effects in dystrophic muscle include sarcolemmal nNOS (48) and membrane excitability (49). Consistency between ex vivo (where blood supply is severed) and in situ results with EDG-5506 suggest that blood perfusion and NOS activity are not essential for protection. Similarly, decreases in force but not calcium in treated lumbrical muscles suggest EDG-5506 does not decrease membrane excitability. Additional studies also explored the promiscuity of EDG-5506 via in vitro binding, enzymatic and phospho-

antibody arrays, confirming low off-target activity for EDG-5506. Regardless, there is still a possibility that other unknown activities of EDG-5506 might contribute to its protective effects.

Protective doses of EDG-5506 had no negative effects on strength, coordination, or habitual activity in mice, suggesting functional accommodation or excess capacity is present in skeletal muscle. Mouse muscles are composed of primarily fast fibers while human muscles are composed of an approximately even split of slow and fast fibers (50). Muscle contraction is controlled by both motor neuron stimulation rate and coordinated recruitment of populations (units) of fast or slow fibers (51). As physical demands increase, stimulation rates and recruitment increases with slow units usually recruiting before faster units (51). This system is designed to maintain physical performance even under extreme stress. Inhibition of fast myosin via EDG-5506 would be expected to reduce fast fiber force but overall muscle performance might still be maintained via force adjustment provided by stimulation and recruitment of motor units. Genetic evidence for both accommodation and adverse effects from total fast fiber inhibition exists in individuals with null mutations in MYH2, the gene encoding myosin IIa which makes up 85% of human fast fibers (52). MHY2-null skeletal muscles have few fast fibers but individuals remain ambulatory although manifest mild to moderate proximal limb and oculofacial weakness and dysfunctional extraocular muscles.

Although selective injury of fast skeletal muscle fibers in DMD was first documented over 30 years ago (13), its cause and relevance to disease progression is poorly understood. Fast fibers differ in many ways from slow fibers that might heighten susceptibility. Possible factors include lower levels of the dystrophin-related protein utrophin (53), lower oxidative and mitochondrial capacity and differences in organization of the z-disc, making it more susceptible to disruption (54). Muscle injury studies in healthy volunteers have shown elevation of circulating troponin I from fast but not slow muscle (55), suggesting that fast fiber sensitivity is perhaps normal physiology amplified in the absence of dystrophin.

Older DMD patients (≥7 yrs.) exhibit muscle fiber dysfunction in both slow and fast fibers including expression of embryonic myosin (17). It is unclear whether fast fiber damage indirectly impacts

slow fibers or whether injury occurs directly over a longer time. One nuance of the biochemical profile of EDG-5506 is that it inhibits both fast and embryonic myosin (Supplemental Table 1). Embryonic myosin, present with fiber regeneration, is present in approximately 30% of DMD patient fibers (56) and should be targeted by EDG-5506, whether they co-express fast or slow myosin. As embryonic myosin is expressed during muscle regeneration, we confirmed that EDG-5506 did not interfere with muscle repair using a cardiotoxin model. A surprising finding of this study was that muscle size was larger with EDG-5506 treatment (Supplemental Figure 7). Young *mdx* mice also undergo large-scale muscle degeneration/regeneration at 3-4 weeks of age (37). EDG-5506 was protective against this degeneration, reducing central nuclei. While neither muscle or fiber size was increased in this study, specific tension was higher than controls and occurred in both *mdx* and WT mice (that exhibit no degeneration). Why myosin inhibition would increase either muscle size or function in these dynamic situations is not currently understood.

Our results in older GRMD also help understanding of compound response in older DMD patients. GRMD exhibit early disease onset that stabilizes at 6 months. Studies in 7-18 month-old GRMD approximates to DMD patients >10 yrs old with muscle weakness and increased occurrence of mixed composition fast/slow fibers (40). In this light, it is encouraging that we observed both decreased CK and increased activity with EDG-5506. There are few precedents for acute functional improvements in GRMD. The closest exemplar in DMD dogs would be glucocorticoids which increased some aspects of physical function and lowered CK (in combination with cyclosporine) but had longer-term adverse effects including muscle atrophy and calcification (57).

Our use of Somascan proteomics on samples from GRMD facilitated a detailed analysis of disease-associated biomarkers in this model. One caveat to this data is that Somascan uses aptamers for human proteins with unknown cross-reactivity against dog. Given this, we saw consistent patterns between GRMD and DMD signatures with overlap between published DMD signatures (43), further validating GRMD as a close comparator to DMD. Treatment with EDG-5506 reversed this overlapping signature, speaking to a universal proteomic correction of disease in GRMD and by

extension, DMD. Limitations of this study include in vivo differences between *mdx*, GRMD and DMD, and the short duration and lack of force measures in our GRMD study.

Our studies demonstrating common beneficial effects of EDG-5506 across preclinical models is unusual and speaks to its fundamental nature. EDG-5506 protects muscle ex vivo and in situ from contraction injury with a response that compares favorably to AAV micro-dystrophin replacement strategies (58, 59). Protection also extended to the heart with lower cardiac fibrosis in DBA/2J *mdx* mice, a finding distinct from AAV micro-dystrophin in the same model (60). Skeletal muscle rescue can improve cardiac health in *mdx* and double knockout dys/utr mice (61). Additional studies will be required to understand cardiac protection with EDG-5506.

In summary, these findings represent an alternative strategy for the treatment of DMD. The mechanism of myosin inhibition is structural in nature and as such is independent of inflammation or the specific genetic lesions conferring disease. As a result, we predict that it should be complimentary with therapeutic approaches that alter inflammation or modify/replace the dystrophin gene such as antisense oligonucleotides or AAV micro-dystrophin. Further studies will explore whether EDG-5506 confers additional therapeutic benefit when combined with glucocorticoids or genetic strategies. Importantly, short-term clinical studies have now been completed in healthy volunteers and individuals with BMD using EDG-5506 (NCT04585464) and longer-term studies are underway in BMD and DMD (NCT05291091, NCT05540860).

Materials and Methods

Actin and myosin S1 preparation. Smooth muscle chicken gizzard S1 was purchased from Cytoskeleton, Inc (Centennial, CO), Other myosin S1 was prepared via published protocols (21). Briefly, fresh rabbit psoas and frozen porcine ventricular muscle (Pel-freez) were extracted in 0.3 M KCl, 0.15 M KH_2PO_4, 1 mM EGTA, 1 mM ATP, 1 mM DTT, pH 6.5 at 4°C. Full-length myosin was purified from each extract via low-ionic precipitations with final precipitation into PM12 buffer (12 mM PIPES, pH 7.0, 2 mM $MgCl_2$). Purified myosin was resuspended in PIPES/EDTA buffer (20

mM PIPES, pH 6.8, 10 mM EDTA, 1 mM DTT) and reacted with 0.2 mg/mL α-chymotrypsin for 30' at RT. Proteolysis was quenched with PMSF (final concentration 100 μM) and the reaction was centrifuged for 45' at 230,000x*g*. S1 fragment in the supernatant was dialyzed into PM12 with 0.02% sodium azide and clarified by centrifugation. Sucrose was added to 10% w/v and flash-frozen in liquid N_2 and stored at -80°C. Actin was purified from minced porcine cardiac muscle after 10' incubation in extraction buffer (0.5 M KCl, 0.1 M K_2HPO_4, pH 7.0). Centrifuged pellets were washed 3-4x with carbonate buffer (Na_2CO_3, pH 8.2-8.5) then 3x with cold acetone. Residues were collected and dried to yield acetone powder. Actin was purified using published methods (21). Actin was polymerized with 0.1 volumes of 10x Polymerization Buffer (50 mM PIPES, pH 7.0, 550 mM KCl, 22 mM EGTA, 22 mM $MgCl_2$, 10 mM ATP), and incubation at RT for 60'.

Myofibril Preparation. Myofibrils were prepared from various animals and tissues: rabbit psoas muscle and porcine cardiac muscle was purchased from Pel-Freez Biologicals (Rogers, AR). Human bicep and soleus muscle were purchased from BioIVT (Westbury, NY) and neonatal rat muscle was a gift from Dr. Leslie Leinwand. All myofibrils were prepared using a published methods (21).

Myofibril and myosin S1 enzymatic activity. A lactate-dehydrogenase/pyruvate-kinase enzyme coupled system (62) was used to monitor ATP hydrolysis rates in various muscle preparations. Rabbit psoas myofibrils were used for high throughput screening at pCa 6.25 at 0.25 mg/mL. A multidrop cassette (Thermofisher Scientific) dispensed 10 μL of the coupled enzyme system, calcium, and myofibrils to 10 μL of ATP, NADH and PEP, to initiate the reaction prior to reading on a plate reader (Envision, Perkin Elmer, Waltham, MA) for 10'/plate at RT. Hits were reconfirmed and secondary assays used to evaluate selectivity, including bovine cardiac myofibrils (pCa 5.86) and enzyme coupled hits with a hexokinase screen (Sigma Aldrich).

Stopped-flow analysis of Pi release from myosin. The rate of Pi release from myosin with actin utilized a fluorescent phosphate binding protein, as described (63). Experiments were performed in 10 mM MOPS pH 7.0; 5 mM KCL; 1 mM EGTA; 1 mM DTT; 0.5 mM $MgCl_2$. ATP/ADP were

removed by incubation with apyrase (64). Prior to mixing with 1 mM ATP in a stopped flow device, compound was incubated with 6 µM psoas S1 at 25ºC for 30'.

Animal Models. C57BL/6 (stock #000664), C57BL/10J (stock #000665, control for *mdx* experiments), C57BL/10ScSn-Dmd^{mdx}/J mice (*mdx*, stock #001801) and D2.B10 (DBA/2-congenic) Dmd^{mdx} mice (DBA/2J *mdx*, stock #013141), were from Jackson Laboratories. Sprague Dawley rats were purchased from Charles River Laboratories. For ex vivo experiments, mice were 10-16 weeks old. For in situ experiments, mice were 8-14 weeks of age. For in vivo chronic dosing studies, mdx and DBA/2J mdx were 4-5 weeks of age at study start. Dosing was via a 10 mL/kg suspension (1% methyl cellulose, 0.1% Tween 80 in water). For studies in 14 day-old pre-weaning mice, PO dosing was via syrup suspension (3 mg/kg/day). GRMD were supplied by Texas A&M Department of Veterinary Integrative Biosciences.

Skinned fiber force measurements. Measurement of isometric force in skinned fibers from rabbit psoas, rat soleus and rat cardiac trabeculae were performed as described (65) with an 802D fiber system (Aurora Scientific). Muscle bundles were thawed from -80°C and placed in relaxing solution. Single fibers were transferred to the testing apparatus with steel pins connected to a force transducer and motor (Model 403A and 322C, Aurora Scientific) and collodion glue applied. Temperature was set to 15°C for skeletal fibers and 30°C for rat cardiac trabeculae, the wells of the 802D were filled with different ratios of relaxing and activating pCa solutions as detailed (65). All control solutions contained 1% final DMSO. Traces were compared between control and compound runs, to evaluate isometric force and calcium sensitivity.

Ex vivo force measurement. Isometric force was measured ex vivo in mouse EDL and SOL muscle. EDL muscle eccentric injury was based on published protocols (30) with degree of lengthening and stimulation modified to yield a uniform drop in mdx isometric and peak force over 10 contractions. After isolation, muscle was mounted via 5-0 suture to a combination servomotor/force transducer (Aurora 300C-LR) between 2 electrodes connected to a stimulator (Aurora 701C) in Ringers solution at 27ºC with continuously infused CO_2/O_2 gas mixture. Experiments were recorded with custom MATLAB software via a National Instruments PCIe-6321

board and 2090A BNC connector. Muscles were pre-incubated for 60' with DMSO (final 0.1%)/compound before 10 eccentric contractions, 1' apart with 100 ms isometric stimulation at 100 Hz and active lengthening of 0.1 L_0 at a rate of 2 L_0/s. After lengthening, muscles were held at 1.1 L_0 with stimulation for 100 ms (Supplemental figure 2A).

For procion imaging, injury protocols were performed in 1% procion MX Dye (020 Brilliant Orange, Jacquard Products) then fixed in cold 4% paraformaldehyde, then cold 30% sucrose/PBS before cryosection. Laminin immunohistochemistry used rabbit polyclonal (Sigma, L9393, 1:20) from Sigma and chicken anti-rabbit Alexa 488 (1:200). slides were scanned at 20x on darkfield with a Nikon Te-2000 and analyzed with Imaris software (Bitplane AG). Imaris' surface component algorithm was used to detect Procion labelled fibers' boundaries. Non-specific procion staining of the peripheral tendon and outer layer of cells (where handling could cause injury) was excluded by applying a size and location filter (>2x average fiber size and located adjacent to laminin positive fibers at the edge of the muscle), Each fiber was identified with an ID and color coded before calculation.

Ex vivo analysis of *mdx* mouse lumbrical muscle contraction, intracellular calcium quantification and isometric injury were described previously (31). Lumbrical muscles were transferred to a custom-built chamber and mounted horizontally to a force transducer (model 400A, Aurora Scientific) at 25^{o}C. Sarcomere length was adjusted to 2.5 µm by microscope. Contraction was elicited with 0.2 ms stimuli and injury via 1s stimuli at 125 Hz.

For fluorescence experiments, a 75W xenon lamp was used with wavelengths selected using a diffraction grating monochromator (Photon Technology International, model DeltaRAM). Muscles were loaded with mag-fura-2 AM (10 µM in Tyrode) for 30' at 25^{o}C and excited at 344 and 375 nm (bandwidth 10 nm) and passed through a 510 nm emission filter (bandwidth 40 nm). Fluorescence responses were recorded alternately during 32 twitch contractions at 20 s intervals, background fluorescence subtracted and the response averaged. High-affinity fura-2 was used to detect membrane breaches between tetanic contractions. Muscles were incubated with fura-2 AM (15 µM

in Tyrode) for 30' before 12 injurious contractions, separated by 1' with (10/s) alternating excitation wavelengths of 340 and 375 nm (bandwidth 1.25 nm) with a 510 nm emission filter (bandwidth 40 nm) and pre-loading backgrounds subtraction. Still and video images were captured using a digital camera (Nikon D750).

In situ force measurement. Measurement of isometric force and eccentric injury response *in situ* was performed in mouse TA muscle based on published protocols (30). Mice were anesthetized with 2% isoflurane (0.7-1.5% maintenance) on a 37°C platform. The distal tendon to the TA and EDL muscle was attached with 4-0 suture a servomotor (Aurora Scientific, ON, Canada). The sciatic nerve was exposed at the knee for hook electrodes. For compound assessment, baseline isometric contraction was assessed at 25-175 Hz (9 mA, 300 ms) followed by 100 Hz stimuli every 5'. After 15', compound was dosed PO and recording continued for 4 hr followed by a second force-frequency. For in situ eccentric injury, compound was administered PO, muscle was stimulated every 5' at 100 Hz for 3.5 hr then two lengthening contractions performed (10' apart, 100 ms at 150 Hz then lengthening 0.2 L_0 at 2 L_0/sec and hold for 100 ms). Isometric force before and 10' after the injury contractions was recorded.

Phosphoprotein array analysis. *mdx* mouse EDL muscle was prepared for ex vivo analysis as described (N=5). Muscles were incubated for 1 hr with DMSO or EDG-5506 (5 µM) then flash frozen in liquid nitrogen. Tissue preparation and analysis was performed as recommended by the manufacturer (https://www.fullmoonbio.com/product/cell-signaling-phospho-antibody-array/).

In vivo assessments in mice. Prior to in vivo assessments, mice were dosed PO post 2-hr fast with 10 mL/Kg suspensions. Grip strength and rotarod assessments were performed blinded, 4-hrs post-dose using published protocols (66, 67). Grip strength was performed with a Columbus Instruments Rodent Force Meter (Columbus, OH). Forepaw strength represented the average of five trials with thirty second rest periods, normalized by BW. Rotarod endurance was performed with a Columbus Instruments RotaMax. Mice were placed on the device drum at 1 rpm, accelerating 1 rpm every 3 sec to 12 rpm and a maximal time of 500 sec, this was repeated 3x with a 3 min rest

and total time reported. Voluntary wheel running performance was assessed with a customized system. Timestamped RPMs were measured 24 hrs/day by infrared sensors and a custom software calculated distance. Whole body Evans blue dye (EBD) was visualized after intravenous administration (35). EBD in PBS at 10 mg/ml was sterile filtered and 50 μl/10 g BW injected via tail vein. After 24 hr, animals were sacrificed, skin removed and fixed in 4% formalin for 24 hr and photographed using a Leica/Lumix camera.

Plasma CK activity. Plasma from mice and dogs was analyzed for CK activity using standard protocols (Pointe Scientific, Thermo Fisher). Note that experiments performed in Supplementary figures 2D and 4B were performed with separated batches of mdx and CK kits and exhibited higher background CK activity compared to previous experiments (Figures 2H, 4B).

Histological and immunohistochemical analysis. For sterile muscle injury, mice were anaesthetized with isoflurane and 50 µl cardiotoxin ($12x10^{-6}$ M, Millipore #217503) injected in the TA muscle. Eight-days post-injury muscles were snap frozen in nitrogen-chilled isopentane. 8 µm cryosections were cut and stained with H&E. For each analysis, >10 slides (per condition/group) containing 6 muscle sections/sample were used and myofibers in the injured area were counted and measured with a Mirax digital scanner and HALO software (68). For adult mouse studies, muscles were fixed in 10% formalin and embedded in paraffin for sectioning. Laminin staining (ThermoFisher Scientific, RB-082) was used to outline fibers and picrosirius red for collagen accumulation. Image analysis was performed using ImarisX64 software (Bitplane AG) and fiber sizing calculated using minimal Feret's diameter **(69)**. For post-weaning juvenile mouse studies, cryosections from soleus muscles were mounted in ProLong™ antifade mountant with DAPI (ThermoFisher). Fiber type, size, and central nucleation was quantified with analysis via SMASH **(70)** and ImageJ. Antibodies used were mouse anti-MHC2A (1:50, https://dshb.biology.uiowa.edu/SC-71) and mouse anti-eMHC (1:10, https://dshb.biology.uiowa.edu/BF-45).

RNAseq analysis of gastrocnemius muscle. RNA sequencing was performed with isolated single nuclei using the 10X Genomics Chromium Single Cell 3' Protocol, Accessories and Kits (CG000183 Rev A). Data was then analyzed by Rosalind (https://rosalind.onramp.bio/), with a HyperScale architecture developed by OnRamp BioInformatics, Inc. (San Diego, CA). Data have been submitted to the Gene Expression Omnibus (GEO) database at the National Institutes of Health (NIH) and are available under accession number GSE227510.

Myosin isoform analysis. Biopsies of dog gastrocnemius muscle (GRMD N=5, Age 6-9 months; WT N=5, Age 6-7 months), rabbit psoas and bovine masseter were snap frozen on liquid nitrogen. Muscle was thawed in lysis buffer (30mM Tris, pH 7.5, 1% SDS) and homogenized in a bead beater for 3' at 3500 rpm. Myosin separating gels were prepared and run as described (71) using 1 µg protein lysate for gastroc and 3.5 µg of psoas/masseter (at 80V for 8 hours then 85V for 18 hours) at 4°C. Protein was quantified using Sypro Total Protein stain (rapid protocol) and visualized on a LiCor Odyssey M. Quantification of fast and slow MHC was performed using Empiria Studio 2.2 software (LiCor, Inc.).

Habitual activity and circulating biomarker measurement in GRMD. Studies were performed in two phases. In the first phase, GRMD (N=4, female, 7 mos old) were dosed PO daily with vehicle for 2 weeks, followed by a suspension of EDG-5506 (3 mg/kg daily for 2 days, then 1 mg/kg daily for two weeks) and finally with vehicle for 2 weeks. Blood was drawn at regular intervals (2-3 draws during the vehicle baseline, 5-8 draws during the dosing period and 2 draws during the vehicle washout). In a separate dosing period, the same four dogs (10 mos old) were administered vehicle for 14 days with regular blood draws (6-9 for each dog across the 14-day period). CK activity (Pointe Scientific, Thermo Fisher) was measured from plasma. In the second phase, the same four dogs (15 mos old) were fitted with a collar-bound activity monitor (Fitbark 2®, Fitbark Inc, Kansas City, MO) as described (42) and baseline activity recorded for 27 days before daily oral gavage with vehicle for 22 days. Three dogs were then dosed in a similar pattern to phase 1 with EDG-5506 (2 mg/kg for 4 days then 2 mg/kg every other day for 7 days). The fourth dog was dosed with vehicle

over the same period. Dogs were then returned to vehicle for a further 12 days. Average daily activity ('Fitbark Points') and time performing various activities (play, rest, active) were recorded.

Somascan® plasma proteomics analysis Somascan (Somalogic, Boulder, CO) protein array (1305 protein analytes for human plasma) was used with dog plasma. Samples were processed according to SomaLogics standard protocols (Plasma_4.3_20180208_1.5k) as described (72). Raw Somascan data were hybridization-control normalized and median-signal normalized and sorted into populations of WT, GRMD baseline, EDG-5506 treatment, and post-dosing washout. Two WT samples were taken from one age-matched healthy littermate. GRMD baseline and EDG-5506 treatment samples were taken from 2 of 4 dogs with 2 GRMD Baseline samples taken/dog the week prior to starting EDG-5506 and treatment samples from 3-4 samples/dog, taken across the treatment period. Two post-dosing washout samples were taken per dog in the week following treatment. Population RFU values were log-transformed to reduce heteroscedasticity, then averaged for every target. Relative concentrations for each target were calculated by subtracting the log-transformed data against that of the WT population. Target comparisons were made using a using a two-tailed t-test, correcting for the false discovery rate using the Benjamini-Hochberg method (73).

Statistical analysis. Unless indicated, results are presented as mean +/- SEM and statistical significance was calculated using one-way ANOVA, two-tailed Student's t-test, or the Kolmogorov-Smirnov test. Where appropriate, p-values have been corrected for multiple comparisons.

Study approval. Mouse procedures at CU Boulder were performed in accordance with and approval of the institutional IACUC (protocol 2589). Sterile injury experiments were carried out in accordance with and approval of the IACUC at Johns Hopkins University (license no: MO18C251). All dogs were used and cared for according to principles outlined in the National Research Council's Guide for the Care and Use of Laboratory Animals. Procedures were approved by the Texas A&M IACUC, protocols 2018–0182 and 2018–0393.

Author contributions:

Conceptualization: AJR, KK, SB, PN, HLS, LAL, SS, KH, LN

Methodology: HMR, CV, DC, BR, KK

Investigation: HMR, MD, BB, YQ, AKP, BLN-S, KH, SS, BR, AVD, CV, YS, DC, AR, AP, YL

Supervision: LN, HLS, AJR, LAL, ERB, KK

Writing – original draft: AJR, BB, AKP

Writing – review & editing: BB, MD, LAL, LN, HLS

Acknowledgments

Thanks go to Peter Thompson and Badreddin Edris for intellectual input, Volker Straub (University of Newcastle) for Evans blue dye advice, Anastasia Karabina (CU Colorado) for help with myosin preparation and Behrad Derakhshan, Marc Evanchik and Joanne Donovan for manuscript review.

References

1. Petrof BJ. The molecular basis of activity-induced muscle injury in Duchenne muscular dystrophy. *Mol Cell Biochem.* 1998;179(1-2):111-23.
2. Gao QQ, and McNally EM. The Dystrophin Complex: Structure, Function, and Implications for Therapy. *Compr Physiol.* 2015;5(3):1223-39.
3. Vandebrouck C, Martin D, Colson-Van Schoor M, Debaix H, and Gailly P. Involvement of TRPC in the abnormal calcium influx observed in dystrophic (mdx) mouse skeletal muscle fibers. *J Cell Biol.* 2002;158(6):1089-96.
4. Burr AR, and Molkentin JD. Genetic evidence in the mouse solidifies the calcium hypothesis of myofiber death in muscular dystrophy. *Cell Death Differ.* 2015;22(9):1402-12.
5. Godi C, Ambrosi A, Nicastro F, Previtali SC, Santarosa C, Napolitano S, et al. Longitudinal MRI quantification of muscle degeneration in Duchenne muscular dystrophy. *Ann Clin Transl Neurol.* 2016;3(8):607-22.
6. Broomfield J, Hill M, Guglieri M, Crowther M, and Abrams K. Life Expectancy in Duchenne Muscular Dystrophy: Reproduced Individual Patient Data Meta-analysis. *Neurology.* 2021;97(23):e2304-e14.
7. Lynch GS, Rafael JA, Chamberlain JS, and Faulkner JA. Contraction-induced injury to single permeabilized muscle fibers from mdx, transgenic mdx, and control mice. *Am J Physiol Cell Physiol.* 2000;279(4):C1290-4.

8. Lindsay A, Baumann CW, Rebbeck RT, Yuen SL, Southern WM, Hodges JS, et al. Mechanical factors tune the sensitivity of mdx muscle to eccentric strength loss and its protection by antioxidant and calcium modulators. *Skelet Muscle.* 2020;10(1):3.
9. Karpati G, Carpenter S, and Prescott S. Small-caliber skeletal muscle fibers do not suffer necrosis in mdx mouse dystrophy. *Muscle Nerve.* 1988;11(8):795-803.
10. Li M, and Arner A. Immobilization of Dystrophin and Laminin alpha2-Chain Deficient Zebrafish Larvae In Vivo Prevents the Development of Muscular Dystrophy. *PLoS One.* 2015;10(11):e0139483.
11. Schiaffino S, and Reggiani C. Myosin isoforms in mammalian skeletal muscle. *J Appl Physiol (1985).* 1994;77(2):493-501.
12. Moens P, Baatsen PH, and Marechal G. Increased susceptibility of EDL muscles from mdx mice to damage induced by contractions with stretch. *J Muscle Res Cell Motil.* 1993;14(4):446-51.
13. Webster C, Silberstein L, Hays AP, and Blau HM. Fast muscle fibers are preferentially affected in Duchenne muscular dystrophy. *Cell.* 1988;52(4):503-13.
14. Barthel BL, Cox D, Barbieri M, Ziemba M, Straub V, Hoffman EP, et al. Elevation of fast but not slow troponin I in the circulation of patients with Becker and Duchenne muscular dystrophy. *Muscle Nerve.* 2021;64(1):43-9.
15. Frohlich T, Kemter E, Flenkenthaler F, Klymiuk N, Otte KA, Blutke A, et al. Progressive muscle proteome changes in a clinically relevant pig model of Duchenne muscular dystrophy. *Sci Rep.* 2016;6:33362.
16. Yuasa K, Nakamura A, Hijikata T, and Takeda S. Dystrophin deficiency in canine X-linked muscular dystrophy in Japan (CXMDJ) alters myosin heavy chain expression profiles in the diaphragm more markedly than in the tibialis cranialis muscle. *BMC Musculoskelet Disord.* 2008;9:1.
17. Marini JF, Pons F, Leger J, Loffreda N, Anoal M, Chevallay M, et al. Expression of myosin heavy chain isoforms in Duchenne muscular dystrophy patients and carriers. *Neuromuscul Disord.* 1991;1(6):397-409.
18. Herrmann C, Sleep J, Chaussepied P, Travers F, and Barman T. A structural and kinetic study on myofibrils prevented from shortening by chemical cross-linking. *Biochemistry.* 1993;32(28):7255-63.
19. Aigner S, Gohlsch B, Hamalainen N, Staron RS, Uber A, Wehrle U, et al. Fast myosin heavy chain diversity in skeletal muscles of the rabbit: heavy chain IId, not IIb predominates. *Eur J Biochem.* 1993;211(1-2):367-72.
20. Bloemberg D, and Quadrilatero J. Rapid determination of myosin heavy chain expression in rat, mouse, and human skeletal muscle using multicolor immunofluorescence analysis. *PLoS One.* 2012;7(4):e35273.
21. Okamoto Y, and Sekine T. A streamlined method of subfragment one preparation from myosin. *J Biochem.* 1985;98(4):1143-5.
22. Shaw MA, Ostap EM, and Goldman YE. Mechanism of inhibition of skeletal muscle actomyosin by N-benzyl-p-toluenesulfonamide. *Biochemistry.* 2003;42(20):6128-35.
23. Kawas RF, Anderson RL, Ingle SRB, Song Y, Sran AS, and Rodriguez HM. A small-molecule modulator of cardiac myosin acts on multiple stages of the myosin chemomechanical cycle. *J Biol Chem.* 2017;292(40):16571-7.
24. Julian FJ. The effect of calcium on the force-velocity relation of briefly glycerinated frog muscle fibres. *J Physiol.* 1971;218(1):117-45.

25. Augusto V, Padovani C, Eduardo G, and Campos R. Skeletal muscle fiber types in C57BL6J mice. *J morphol Sci.* 2004;21(2):89-94.
26. Blaauw B, Mammucari C, Toniolo L, Agatea L, Abraham R, Sandri M, et al. Akt activation prevents the force drop induced by eccentric contractions in dystrophin-deficient skeletal muscle. *Hum Mol Genet.* 2008;17(23):3686-96.
27. Barton ER, Morris L, Musaro A, Rosenthal N, and Sweeney HL. Muscle-specific expression of insulin-like growth factor I counters muscle decline in mdx mice. *J Cell Biol.* 2002;157(1):137-48.
28. Demonbreun AR, Fallon KS, Oosterbaan CC, Vaught LA, Reiser NL, Bogdanovic E, et al. Anti-latent TGFbeta binding protein 4 antibody improves muscle function and reduces muscle fibrosis in muscular dystrophy. *Sci Transl Med.* 2021;13(610):eabf0376.
29. Dellorusso C, Crawford RW, Chamberlain JS, and Brooks SV. Tibialis anterior muscles in mdx mice are highly susceptible to contraction-induced injury. *J Muscle Res Cell Motil.* 2001;22(5):467-75.
30. Petrof BJ, Shrager JB, Stedman HH, Kelly AM, and Sweeney HL. Dystrophin protects the sarcolemma from stresses developed during muscle contraction. *Proc Natl Acad Sci U S A.* 1993;90(8):3710-4.
31. Claflin DR, and Brooks SV. Direct observation of failing fibers in muscles of dystrophic mice provides mechanistic insight into muscular dystrophy. *Am J Physiol Cell Physiol.* 2008;294(2):C651-8.
32. Allen DG, Whitehead NP, and Froehner SC. Absence of Dystrophin Disrupts Skeletal Muscle Signaling: Roles of Ca2+, Reactive Oxygen Species, and Nitric Oxide in the Development of Muscular Dystrophy. *Physiol Rev.* 2016;96(1):253-305.
33. Acakpo-Satchivi LJ, Edelmann W, Sartorius C, Lu BD, Wahr PA, Watkins SC, et al. Growth and muscle defects in mice lacking adult myosin heavy chain genes. *J Cell Biol.* 1997;139(5):1219-29.
34. Wooddell CI, Zhang G, Griffin JB, Hegge JO, Huss T, and Wolff JA. Use of Evans blue dye to compare limb muscles in exercised young and old mdx mice. *Muscle Nerve.* 2010;41(4):487-99.
35. Straub V, Rafael JA, Chamberlain JS, and Campbell KP. Animal models for muscular dystrophy show different patterns of sarcolemmal disruption. *J Cell Biol.* 1997;139(2):375-85.
36. Stedman HH, Sweeney HL, Shrager JB, Maguire HC, Panettieri RA, Petrof B, et al. The mdx mouse diaphragm reproduces the degenerative changes of Duchenne muscular dystrophy. *Nature.* 1991;352(6335):536-9.
37. DiMario JX, Uzman A, and Strohman RC. Fiber regeneration is not persistent in dystrophic (MDX) mouse skeletal muscle. *Dev Biol.* 1991;148(1):314-21.
38. Fukada S, Morikawa D, Yamamoto Y, Yoshida T, Sumie N, Yamaguchi M, et al. Genetic background affects properties of satellite cells and mdx phenotypes. *Am J Pathol.* 2010;176(5):2414-24.
39. van Putten M, Putker K, Overzier M, Adamzek WA, Pasteuning-Vuhman S, Plomp JJ, et al. Natural disease history of the D2-mdx mouse model for Duchenne muscular dystrophy. *FASEB J.* 2019;33(7):8110-24.
40. Kornegay JN. The golden retriever model of Duchenne muscular dystrophy. *Skelet Muscle.* 2017;7(1):9.
41. Valentine BA, Blue JT, and Cooper BJ. The effect of exercise on canine dystrophic muscle. *Ann Neurol.* 1989;26(4):588.

42. Rutledge AM, Guo LJ, Lord LE, Leal AR, Deramus J, Lopez SM, et al. Comprehensive assessment of physical activity correlated with muscle function in canine Duchenne muscular dystrophy. *Ann Phys Rehabil Med.* 2021:101611.
43. Hathout Y, Liang C, Ogundele M, Xu G, Tawalbeh SM, Dang UJ, et al. Disease-specific and glucocorticoid-responsive serum biomarkers for Duchenne Muscular Dystrophy. *Sci Rep.* 2019;9(1):12167.
44. Gyimesi M, Horvath AI, Turos D, Suthar SK, Penzes M, Kurdi C, et al. Single Residue Variation in Skeletal Muscle Myosin Enables Direct and Selective Drug Targeting for Spasticity and Muscle Stiffness. *Cell.* 2020;183(2):335-46 e13.
45. Dahlqvist JR, Voss LG, Lauridsen T, Krag TO, and Vissing J. A pilot study of muscle plasma protein changes after exercise. *Muscle Nerve.* 2014;49(2):261-6.
46. Getz EB, Cooke R, and Lehman SL. Phase transition in force during ramp stretches of skeletal muscle. *Biophys J.* 1998;75(6):2971-83.
47. Rassier DE, and Herzog W. Relationship between force and stiffness in muscle fibers after stretch. *J Appl Physiol (1985).* 2005;99(5):1769-75.
48. Rebolledo DL, Kim MJ, Whitehead NP, Adams ME, and Froehner SC. Sarcolemmal targeting of nNOSmu improves contractile function of mdx muscle. *Hum Mol Genet.* 2016;25(1):158-66.
49. Call JA, Warren GL, Verma M, and Lowe DA. Acute failure of action potential conduction in mdx muscle reveals new mechanism of contraction-induced force loss. *J Physiol.* 2013;591(15):3765-76.
50. Saltin BG, P.D. Skeletal muscle adaptability: significance for metabolism and performance. *Handbook of Physiology; Peachey, LD Ed.* 1983:555-631.
51. Freund HJ. Motor unit and muscle activity in voluntary motor control. *Physiol Rev.* 1983;63(2):387-436.
52. Tajsharghi H, Hammans S, Lindberg C, Lossos A, Clarke NF, Mazanti I, et al. Recessive myosin myopathy with external ophthalmoplegia associated with MYH2 mutations. *Eur J Hum Genet.* 2014;22(6):801-8.
53. Chakkalakal JV, Stocksley MA, Harrison MA, Angus LM, Deschenes-Furry J, St-Pierre S, et al. Expression of utrophin A mRNA correlates with the oxidative capacity of skeletal muscle fiber types and is regulated by calcineurin/NFAT signaling. *Proc Natl Acad Sci U S A.* 2003;100(13):7791-6.
54. Friden J, Sjostrom M, and Ekblom B. Myofibrillar damage following intense eccentric exercise in man. *Int J Sports Med.* 1983;4(3):170-6.
55. Chapman DW, Simpson JA, Iscoe S, Robins T, and Nosaka K. Changes in serum fast and slow skeletal troponin I concentration following maximal eccentric contractions. *J Sci Med Sport.* 2013;16(1):82-5.
56. Janghra N, Morgan JE, Sewry CA, Wilson FX, Davies KE, Muntoni F, et al. Correlation of Utrophin Levels with the Dystrophin Protein Complex and Muscle Fibre Regeneration in Duchenne and Becker Muscular Dystrophy Muscle Biopsies. *PLoS One.* 2016;11(3):e0150818.
57. Barthelemy I, Uriarte A, Drougard C, Unterfinger Y, Thibaud JL, and Blot S. Effects of an immunosuppressive treatment in the GRMD dog model of Duchenne muscular dystrophy. *PLoS One.* 2012;7(11):e48478.
58. Foster H, Sharp PS, Athanasopoulos T, Trollet C, Graham IR, Foster K, et al. Codon and mRNA sequence optimization of microdystrophin transgenes improves expression and

physiological outcome in dystrophic mdx mice following AAV2/8 gene transfer. *Mol Ther.* 2008;16(11):1825-32.
59. Harper SQ, Hauser MA, DelloRusso C, Duan D, Crawford RW, Phelps SF, et al. Modular flexibility of dystrophin: implications for gene therapy of Duchenne muscular dystrophy. *Nat Med.* 2002;8(3):253-61.
60. Hakim CH, Wasala NB, Pan X, Kodippili K, Yue Y, Zhang K, et al. A Five-Repeat Micro-Dystrophin Gene Ameliorated Dystrophic Phenotype in the Severe DBA/2J-mdx Model of Duchenne Muscular Dystrophy. *Mol Ther Methods Clin Dev.* 2017;6:216-30.
61. Crisp A, Yin H, Goyenvalle A, Betts C, Moulton HM, Seow Y, et al. Diaphragm rescue alone prevents heart dysfunction in dystrophic mice. *Hum Mol Genet.* 2011;20(3):413-21.
62. De La Cruz EM, and Ostap EM. Kinetic and equilibrium analysis of the myosin ATPase. *Methods Enzymol.* 2009;455:157-92.
63. White HD, Belknap B, and Webb MR. Kinetics of nucleoside triphosphate cleavage and phosphate release steps by associated rabbit skeletal actomyosin, measured using a novel fluorescent probe for phosphate. *Biochemistry.* 1997;36(39):11828-36.
64. De La Cruz EM, Wells AL, Rosenfeld SS, Ostap EM, and Sweeney HL. The kinetic mechanism of myosin V. *Proc Natl Acad Sci U S A.* 1999;96(24):13726-31.
65. Roche SM, Gumucio JP, Brooks SV, Mendias CL, and Claflin DR. Measurement of Maximum Isometric Force Generated by Permeabilized Skeletal Muscle Fibers. *J Vis Exp.* 2015(100):e52695.
66. Gilli F, Royce DB, and Pachner AR. Measuring Progressive Neurological Disability in a Mouse Model of Multiple Sclerosis. *J Vis Exp.* 2016(117).
67. Luca AD. Use of grip strength meter to assess the limb strength of *mdx* mice. *TREAT-NMD Neuromusclar Network, DMD_M22(20).* 2008:1-11.
68. Patsalos A, Pap A, Varga T, Trencsenyi G, Contreras GA, Garai I, et al. In situ macrophage phenotypic transition is affected by altered cellular composition prior to acute sterile muscle injury. *J Physiol.* 2017;595(17):5815-42.
69. Briguet A, Courdier-Fruh I, Foster M, Meier T, and Magyar JP. Histological parameters for the quantitative assessment of muscular dystrophy in the mdx-mouse. *Neuromuscul Disord.* 2004;14(10):675-82.
70. Smith LR, and Barton ER. SMASH - semi-automatic muscle analysis using segmentation of histology: a MATLAB application. *Skelet Muscle.* 2014;4:21.
71. Warren CM, and Greaser ML. Method for cardiac myosin heavy chain separation by sodium dodecyl sulfate gel electrophoresis. *Anal Biochem.* 2003;320(1):149-51.
72. Kim CH, Tworoger SS, Stampfer MJ, Dillon ST, Gu X, Sawyer SJ, et al. Stability and reproducibility of proteomic profiles measured with an aptamer-based platform. *Sci Rep.* 2018;8(1):8382.
73. Benjamini Y, and Hochberg Y. Controlling the False Discovery Rate: A Practical and Powerful Approach to Multiple Testing. *Journal of the Royal Statistical Society Series B (Methodological).* 1995;57(1):289-300.
74. Marian AJ. On mice, rabbits, and human heart failure. *Circulation.* 2005;111(18):2276-9.
75. d'Albis A, Couteaux R, Janmot C, and Roulet A. Specific programs of myosin expression in the postnatal development of rat muscles. *Eur J Biochem.* 1989;183(3):583-90.
76. Houdusse A, and Sweeney HL. How Myosin Generates Force on Actin Filaments. *Trends Biochem Sci.* 2016;41(12):989-97.

Figures and Tables

Figure 1.

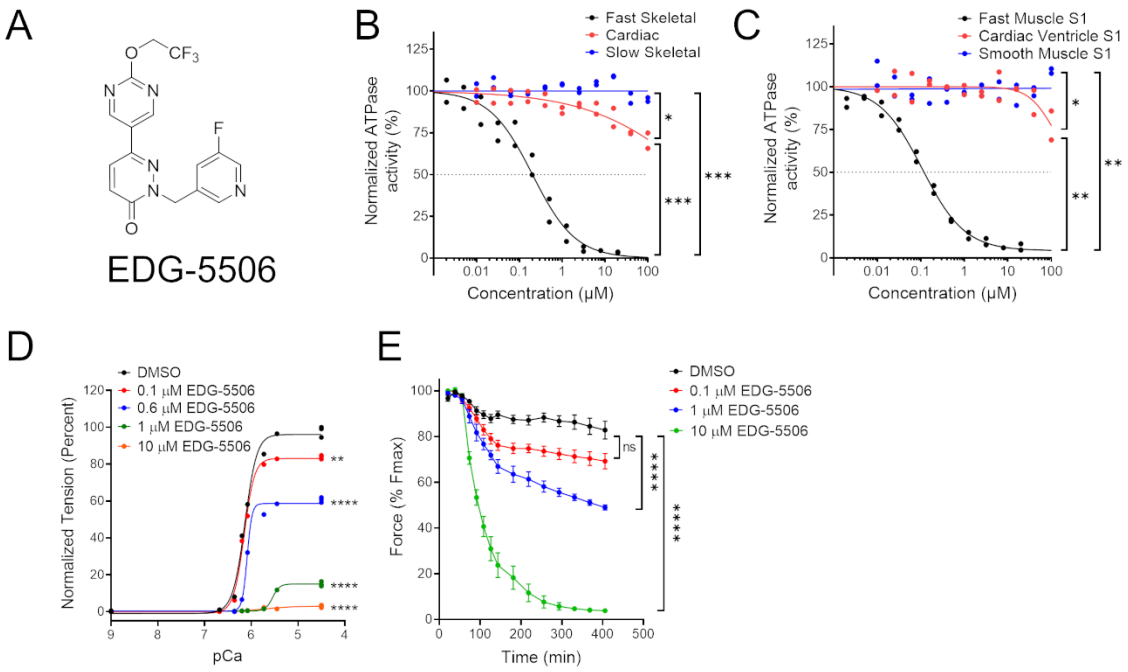

EDG-5506 is a selective inhibitor of fast skeletal myosin ATPase and force generation in fast skeletal muscle. (A) Chemical structure of EDG-5506. (B) Myofibril ATPase activity curves for EDG-5506 with myofibrils isolated from rabbit fast skeletal muscle, bovine cardiac ventricle and slow bovine masseter muscle. (C) Purified myosin S1 ATPase activity curves for EDG-5506 with rabbit fast skeletal muscle (psoas muscle), pig cardiac muscle and smooth muscle myosin S1, isolated from chicken gizzard. ATPase activity in the myofibrils is measured at the pCa50 value for free calcium for each muscle type (N=2). (D) Representative force-calcium curve in single permeabilized fast skeletal muscle fibers (rabbit psoas) with EDG-5506. (E) Percent of initial force with time after addition of EDG-5506 in WT mouse EDL muscle *ex vivo*. Force was recorded at 250 Hz. Each point represents mean peak force +/- 1 SEM (N=4).

Figure 2.

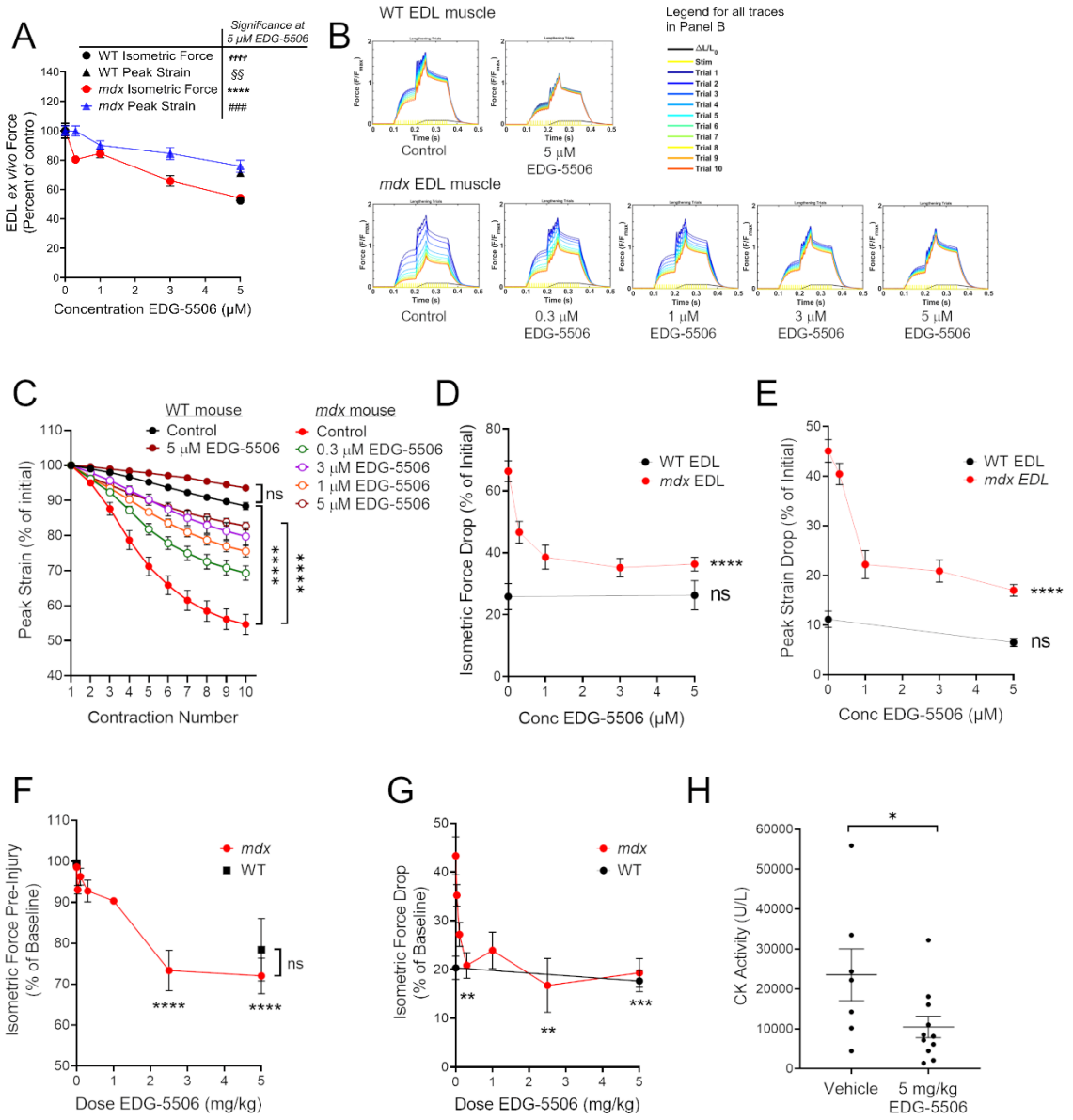

Strength loss during eccentric contraction of dystrophic muscle is dependent upon contraction via myosin. (A) to (E), WT and mdx mouse EDL muscle force ex vivo (N=5-14). (A) Change in isometric and peak strain as a function of EDG-5506 concentration. Change in isometric force (circles) is represented as a percent of initial force after 1 hr incubation with EDG-5506. Significance calculated from the comparison of 5 μM EDG-5506 vs control. Peak strain (triangles) is represented as a percent of peak strain obtained with vehicle treatment derived from the first eccentric contraction. Definitions of these metrics are provided in Supplemental Figure 2A. (B) Example force traces during 10 lengthening contractions of mdx and WT mouse EDL muscle ex vivo after incubation with the indicated concentrations of EDG-5506. (C) Normalized peak strain with each contraction of the injury protocol (N=4-8). (D) Isometric force drop from the first to the last contraction as a function of EDG-5506 concentration. (E) Peak strain drop from the first to the last contraction as a function of EDG-5506 concentration. (F) to (H) WT and mdx mouse TA muscle

force in situ (WT N=6, mdx vehicle N=17, mdx EDG-5506 N=3-5 each). (F) Change in isometric force as a function of EDG-5506 dose, represented as a percent of initial force 3 hr after oral gavage of vehicle or EDG-5506. (G) Isometric force drop 10 min after two lengthening contractions, represented as a percent of pre-injury force. All indicated comparisons are made again zero EDG-5506. (H) CK activity one-hour post in situ injury (N=7-11). Graphs show mean +/- SEM. Significance calculated by one-way ANOVA with Dunnet's multiple comparison (*<0.05; **<0.01; ***<0.001; ****<0.0001. Similar for §, #, and † symbols). Dose-response comparisons compare specific concentration to zero EDG-5506.

Figure 3.

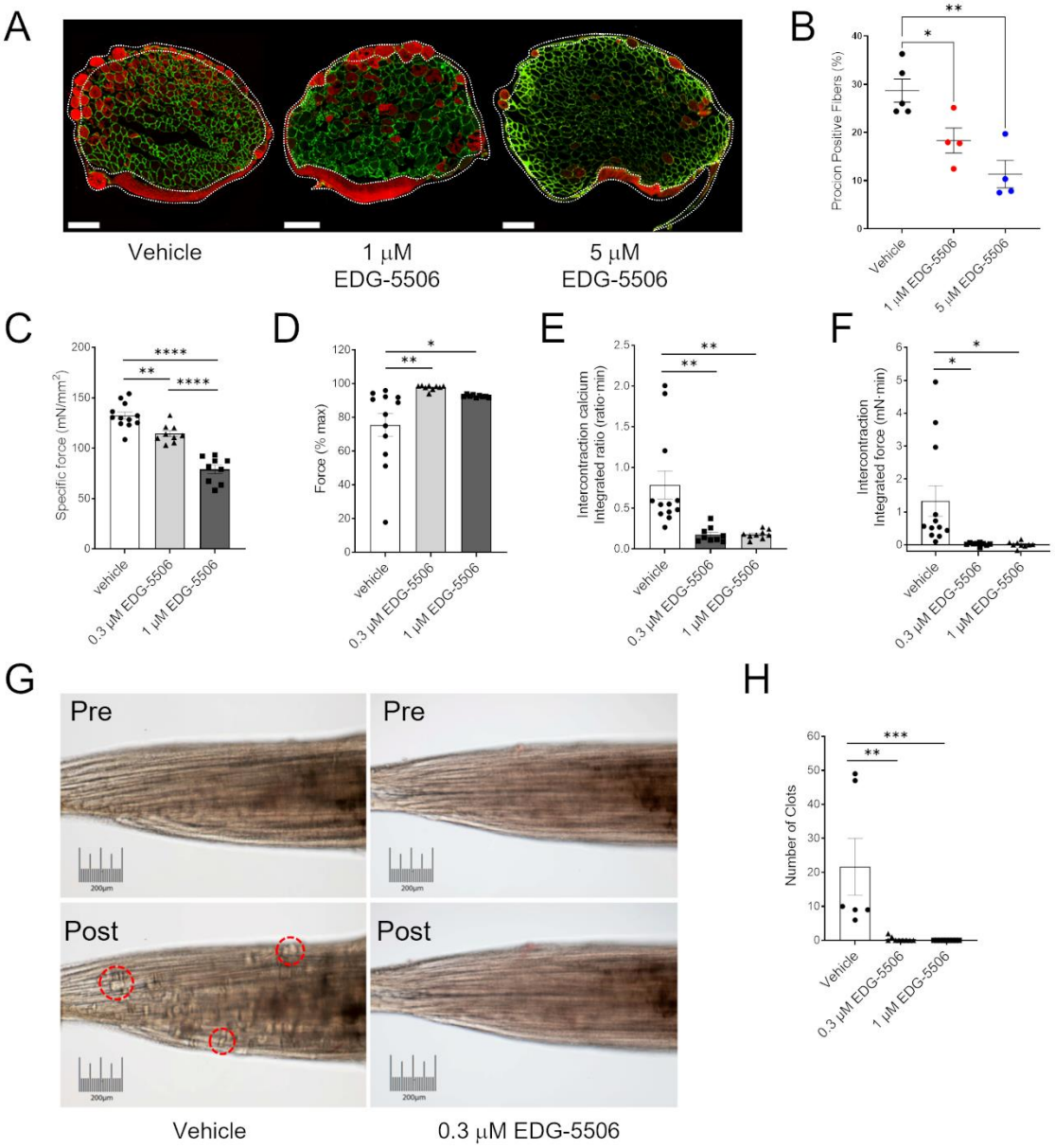

Membrane injury arising from contraction of dystrophic muscle is dependent upon contraction via myosin. (A) Representative immunofluorescence images of procion orange-positive fibers after eccentric contraction in *mdx* EDL muscle. Green channel laminin, red channel procion orange (N=4). Scale, 200 μm. White dotted areas indicate possible non-specific staining that was excluded during analysis. (B) Quantification of procion positive fibers. (C) Specific force prior to injury in *mdx* lumbrical muscles after 1 hr incubation with EDG-5506. (D) Force change from the first to the last repeated tetanic contraction of *mdx* lumbrical muscles. (E) Average inter-contraction fura-2 fluorescence ratio during repeated tetanic contraction. (F) Average inter-contraction force during repeated tetanic contraction. (G) Representative muscle images after 12 contractions. Example clots highlighted in red. (H) Quantification of muscle clots from retracted

fibers (N=8-12). Errors +/- SEM. Significance calculated by one-way ANOVA with Dunnet's multiple comparison (*<0.05; **<0.01; ***<0.001; ****<0.0001).

Figure 4.

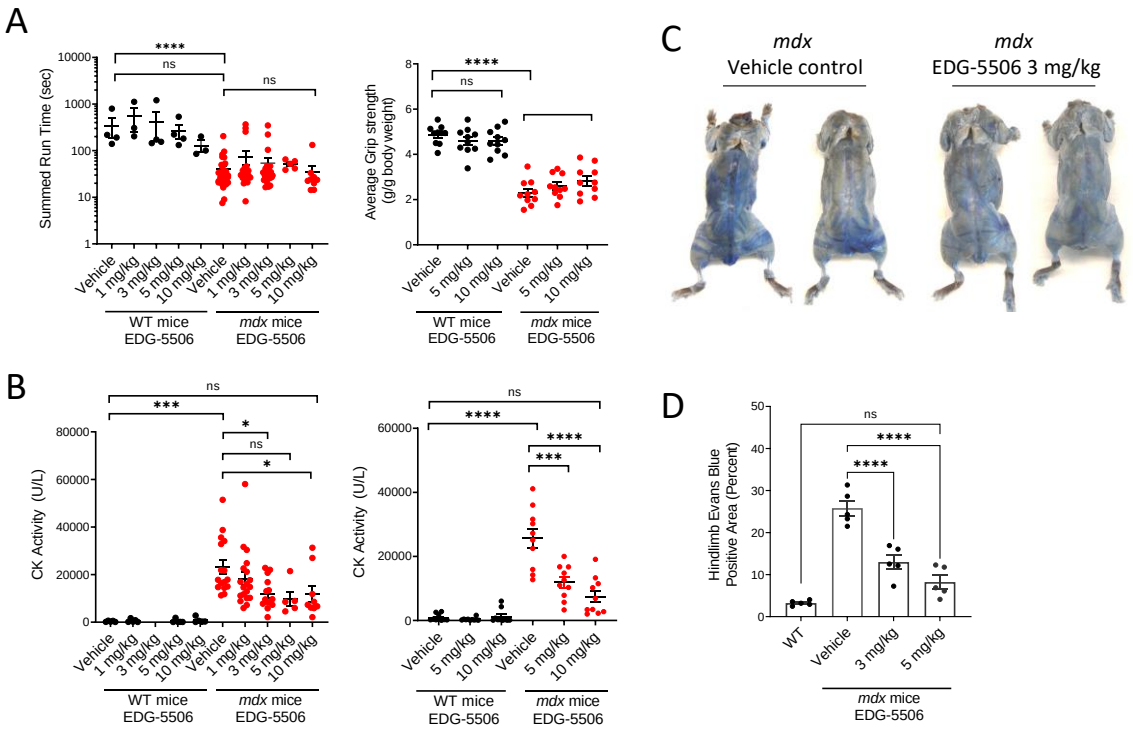

Normalization of membrane permeability with EDG-5506 in *mdx* mice without detrimental effects on strength and coordination in vivo. (A) Left, rotarod performance. Right, forelimb grip strength 4 hr after oral administration of EDG-5506 (N=10-31). (B) Plasma CK activity from blood taken 1 hr after rotarod (left) or grip strength tests (right) (N=10-19). (C) Representative whole-body images of non-exercised *mdx* mice 24 hrs after intravenous administration of Evans blue dye. Mice were treated for three weeks with vehicle or EDG-5506 (these images are reproduced as part of supplement figure 4C). (D) Quantitation of Evans blue dye-positive area in the hindlimbs of treated mice (N=5). (1-10 mg/kg represents approx. 0.079-0.79 μmol EDG-5506/mouse) Significance calculated by one-way ANOVA with Dunnet's multiple comparison (*<0.05; **<0.01; ***<0.001; ****<0.0001).

Figure 5.

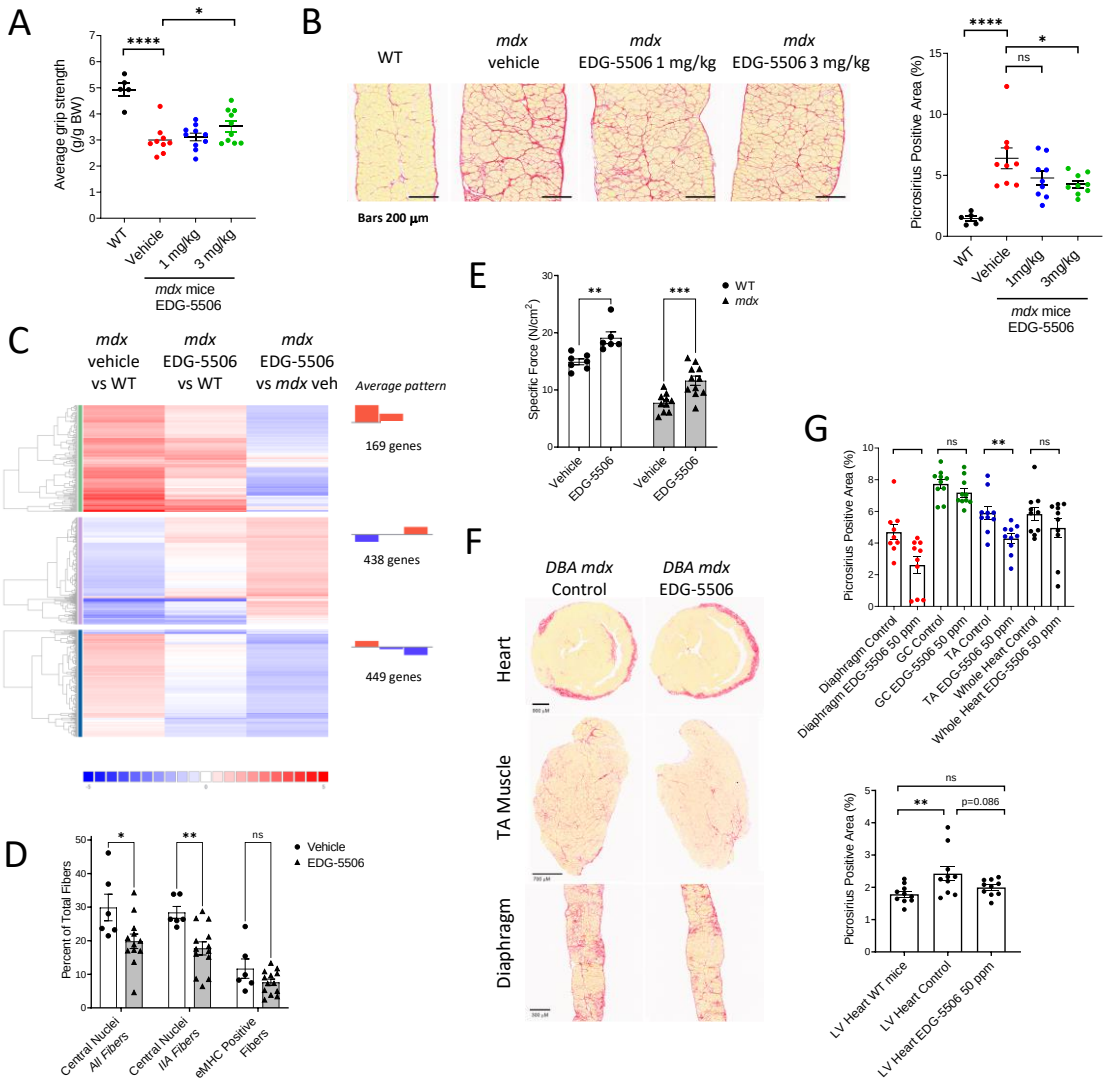

Longer term exposure of protective levels of myosin inhibition are sufficient to decrease muscle degeneration and fibrosis in *mdx* mice. (A) Average grip strength (experimenter-blinded) measured after 5 weeks dosing in *mdx* mice (N=5-10). (B) Left, representative images. Right, quantification of collagen (stained with picrosirius red) in *mdx* mouse diaphragm after 8 weeks treatment (N=9-10). (C) RNA-seq meta-analysis. Colors graded by $\log_2$ fold change (WT N=2, *mdx* vehicle, EDG-5506 N=3). (D) Histological quantification of central nuclei and eMHC positive fibers in soleus muscle sections from post-weaning *mdx* mice after 3 weeks EDG-5506 administration. (E) Specific force in the soleus muscle *ex vivo* in post-weaning mdx and WT mice after 3-weeks treatment with EDG-5506 or vehicle. (F) Representative histology sections examining muscle fibrosis in DBA/2 *mdx* mice after 12 weeks treatment with control or EDG-5506 chow (50 ppm or 0.13 mmol/Kg chow). (G) Quantification of collagen (picrosirius red area). Top, collagen quantification in select muscles (GC, gastrocnemius; TA, anterior tibialis). Bottom, collagen quantification in the left ventricle (N=9-10). Error bars shown +/- SEM. Significance calculated by one-way ANOVA with Dunnet's multiple comparison. *p<0.05; ** p<0.01; ***<0.001; **** p<0.0001.

Figure 6.

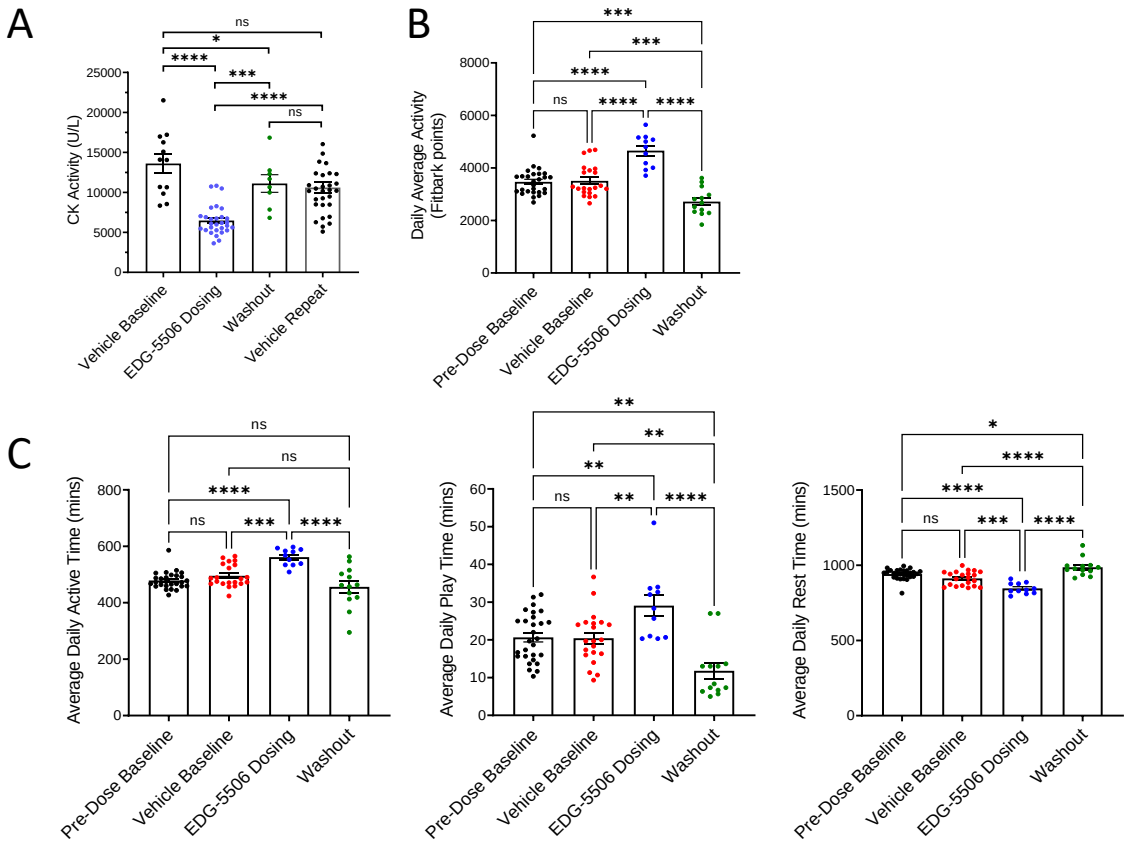

Selective inhibition of active contraction in fast skeletal muscle decreases CK and increases habitual activity in DMD dogs. (A) Plasma CK activity in 7-month-old DMD dogs (N=4) before, during, and after 14 days oral gavage with EDG-5506. Each datapoint represents CK activity from an individual blood draw (2-3 draws during the vehicle baseline, 5-8 draws during the dosing period and 2 draws during the vehicle washout). In a separate study, the same 4 dogs were dosed daily with vehicle and blood CK was at regular intervals for 14 days (indicated as vehicle repeat, 6-9 blood draws per dog). Error bars shown +/- SEM. (B) Average daily activity measures from an electronic activity monitor (FitBark®) in the same DMD dogs (N=3, 15 mos old) before, during and after 11 days oral gavage with EDG-5506 (2 mg/kg daily for four days then every other day). Each datapoint represents the daily average activity for the 3 dogs. (C) Timed function data from the same activity monitors. Average daily active time, average daily play time, and average daily rest time. Each point represents one day's average activity. (2 mg/kg represents approx. 68.2 μmol EDG-5506/dog). Significance calculated by one-way ANOVA with Tukey's multiple comparison correction. In all panels: * p<0.05, **p<0.01, ***p<0.001, ****p<0.0001.

Figure 7.

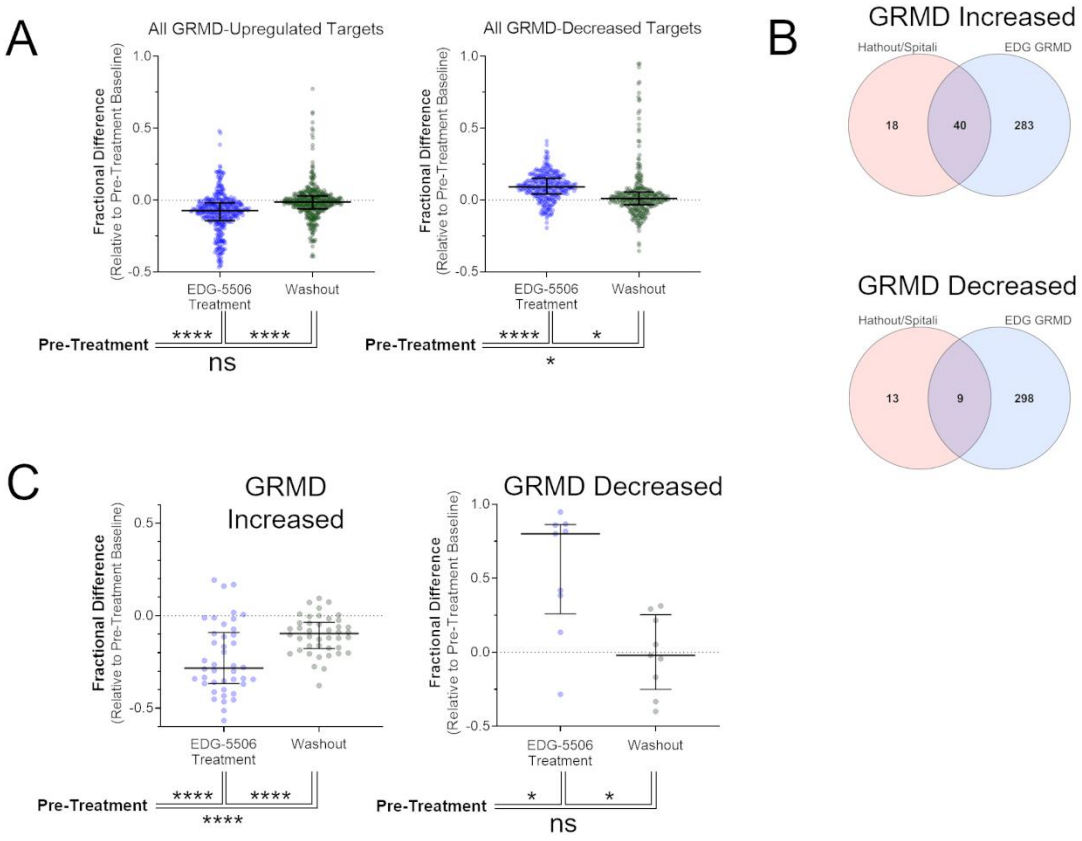

Selective inhibition of contraction in fast skeletal muscle reverses proteomic signatures associated with disease in DMD dogs. (A) Effect of EDG-5506 treatment on plasma proteins identified by Somascan as increased (left) or decreased (right) in DMD dogs compared to healthy littermates. Fractional change was then calculated for each target during the treatment and washout period, relative to the pre-dose baseline. Error bars shown as median +/- interquartile range. (B) Overlap of GRMD increased and decreased proteins with those from a common DMD patient dataset (43). (C) Effect of treatment with EDG-5506 on common DMD elevated (left) or reduced (right) proteins. Error bars show median +/- interquartile range. See supplementary data 3 for full analysis. Significance calculated by one-way ANOVA with Tukey's multiple comparison correction. In all panels: * p<0.05, **p<0.01, ***p<0.001, ****p<0.0001.